J. COMBIN. MATH. COMBIN. COMPUT. 125a (2025) 8105--8117

Journal of Combinatorial Mathematics
and Combinatorial Computing
www.combinatorialpress.com/jcmcc

Combinatorial Press

YOLO-R Computer Key Technology for Trackside Equipment Information Recognition and Detection

Duanyang Cai[1], Huafeng Zhuge[1], Ru Wang[1,✉], Cong Wu[1], Guo Zhang[2]

[1] *Zhejiang Haining Rail Transit Operation Management Co., Ltd., Haining, Zhejiang, 314400, China*
[2] *Chengdu Tangyuan Electric Co., Ltd., Chengdu, Sichuan, 610000, China*

ABSTRACT
With the rapid expansion of high-speed railway network, the real-time monitoring of trackside equipment becomes particularly important. To detect trackside equipment information more accurately, a YOLO-R algorithm grounded on the improved You Only Look Once v3 (YOLOv3) algorithm is proposed, and the trackside equipment identification and detection model is constructed. By introducing feature pyramid network and adaptive Bessel curve network, the new model can effectively identify and locate different types of trackside equipment such as switch machine, derailer, and shaft counter. The experiment findings denote that the new model is superior to the existing technology in all aspects of on-orbit equipment recognition and detection, the computer resource occupancy rate is only 22%, the image recognition accuracy rate is more than 98%, and the processing speed is up to 200 images/second. This research not only raises the automation level of trackside equipment monitoring, but also provides a powerful technology for railway safety operation.

Keywords: YOLOv3, Trackside equipment, Image recognition, Image processing, Feature pyramid network

1. Introduction

China's high-speed railroad technology also began to develop rapidly in the third stage, high-speed railroad has also become a particularly complex operating system, mainly the railroad system and signaling system, any one of these two systems will affect the normal operation of the train if there is a problem in any one of these two systems, high-speed railroads are very demanding on all aspects of the system's construction and maintenance [1-3]. One of the most basic is the train track and trackside equipment and instruments, each module is complementary to each other and plays a vital role in the transportation business of the railroad [4-6].

✉ Corresponding author.
E-mail address: 17853291705@163.com (R. Wang).
Received 25 January 2024; Revised 10 April 2024; Accepted 25 November 2024; Published Online 15 April 2025.
DOI: 10.61091/jcmcc127a-446

Good tracks and equipment are the most basic prerequisite to ensure the high-speed and safe operation of trains. Since the railroad tracks are generally laid outdoors and in sparsely populated places, with the passage of time and the influence of the harsh environment, it may cause fatal impacts on the railroad tracks or trackside equipments, and in serious cases, it will cause unimaginable threats to the safety of train operation [7-10]. In order to better monitor and maintain the train along the line, China independently developed a high-speed railroad special comprehensive inspection car, as the railroad equipment "medical checkup instrument", the infrastructure generally need to carry out a period of about half a month inspection cycle, is a high-speed train safe operation of the behind-the-scenes umbrella. Train tracks for comprehensive system testing [11-13].

In recent years, with the wide application of artificial intelligence technology in various industries, the integration of AI intelligent construction has gradually become an inevitable trend in the transformation and upgrading of rail transportation construction [14-15]. Signal engineering is one of the "four electric" projects of the railroad, which needs to determine the installation position of trackside equipment such as signaling machines and measure the limit data. The traditional manual on-site survey method has problems such as poor measurement accuracy and low labor efficiency, which is also not conducive to the comprehensive digital transformation of the "four electric" projects in the future [16-18].

Based on this, a Trackside Equipment Identification and Detection Model (TEID) grounded on the You Only Look Once v3 Refined (YOLO-R) algorithm was proposed, which innovatively integrates LightenNet and Multi-Band Lighting and Enhancement Network (MBLLEN) image preprocessing techniques to reduce the impact of environmental light changes on detection performance. It is imperative to strengthen the model's capacity to detect small targets and improve detection accuracy by innovatively improving the backbone network. Meanwhile, the Adaptive Bezier Curve Network (ABCNet) was introduced to optimize the numbering of trackside equipment, to improve the model's recognition ability for arbitrary shaped text and solve the problem of insufficient recognition ability of traditional methods in complex backgrounds and occlusion situations.

2. Method

2.1. Improvement of YOLOv3 algorithm

Ensuring the safety and reliability of the track and its surrounding equipment is crucial to the rapid development of high-speed rail. The YOLOv3 algorithm is broadly utilized in object detection due to its fast speed and good performance. However, YOLOv3 has poor detection capabilities for small targets such as trackside equipment in the complex environment of high-speed rail tracks, making it difficult to meet the requirements. To raised the detection efficiency and accuracy of trackside equipment, the study adopts an improved YOLOv3 algorithm YOLO-R algorithm to detect equipment next to high-speed rail tracks. The YOLO-R algorithm structure is denoted in Figure 1.

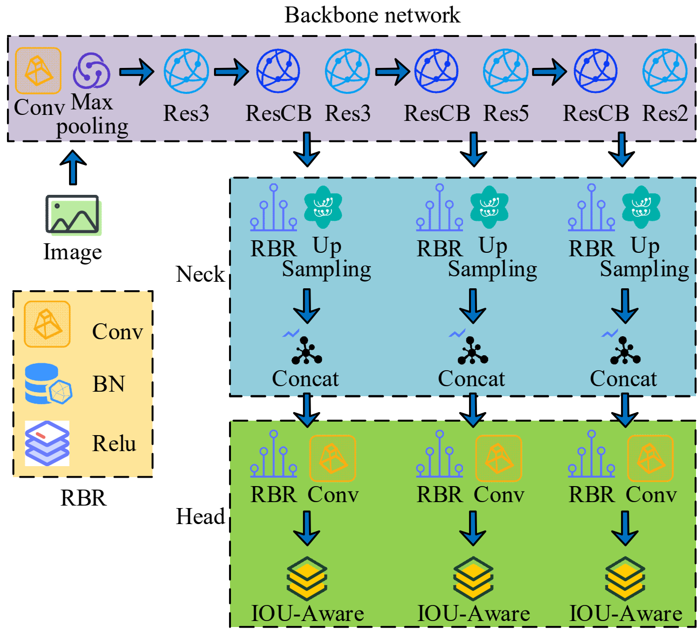

Fig. 1. YOLO-R structure

As illustrated in Figure 1, the YOLO-R structure comprises three components: the backbone network, the neck, and the head. The function of the backbone network is to extract feature information from images of the input trackside device. ResNet50 is formed by stacking multiple residual blocks, with each residual block consisting of two convolutional layers. The backbone network of YOLO-R has been changed from Darknet-53 to ResNet50 to effectively alleviate gradient vanishing and exploding problems, while also having strong scalability. The structure of ResNet50 is shown in Figure 2.

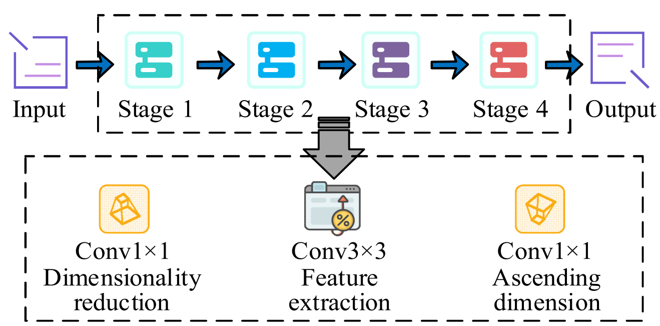

Fig. 2. ResNet50 structure

In Figure 2, the ResNet50 deep residual network structure contains three main parts: input, residual blocks in four stages, and output. Stage 1 to Stage 4 consist of multiple Bottlenecks. There are shortcut connections between each Bottleneck, allowing input to skip certain layers directly to solve the issue of gradient vanishing in deep networks. The function of the neck structure is to collect multi-scale trackside device images captured by the backbone network and integrate image feature parameters. YOLO-R adds 4× downsampling feature maps on the basis of YOLOv3 to preserve small object details and improve detection accuracy. Feature Pyramid Networks (FPN) can enhance YOLO-R's detection capability for targets of different sizes. The FPN allows for more detailed information to be captured from lower level feature maps, and for more semantic information to be captured from higher level feature maps, thus improving the detection accuracy of YOLO-R for small-sized trackside components. The FPN structure is shown in Figure 3.

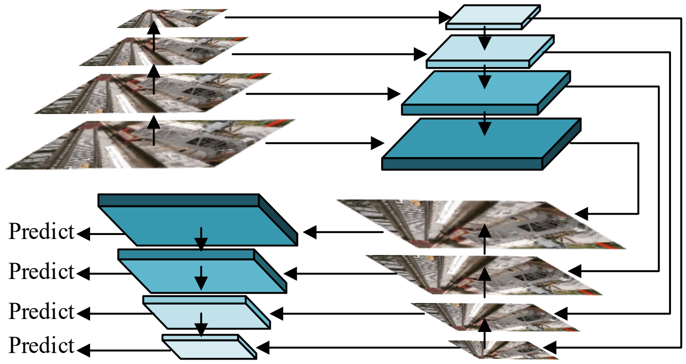

Figu. 3. Structure of FPN

In Figure 3, FPN is a structure used to construct multi-scale feature representations. FPN generates a multi-scale feature pyramid by combining deep and shallow trackside device feature maps. Bottom-up paths, top-down paths and lateral connections are the main components of FPN. The calculation formula for horizontal connection is shown in equation (1).

$$P_{merged} = P_{lateral} + Upsample(P_{top}) \tag{1}$$

P_{merged} represents the merged trackside equipment feature map, $P_{lateral}$ represents the horizontally connected trackside equipment feature map, and $P_{lateral}$ represents the upper level trackside equipment feature map after adoption. The calculation formula for mapping the FPN prediction results to the trackside equipment feature map is shown in equation (2).

$$t\arg et_l vls = floor(lvl0 + \log_2\left(\frac{s}{s_0}\right) + \varepsilon) \tag{2}$$

$t\arg et_l vls$ represents the target scale of feature maps at different levels and s is the square root of the predicted area, s_0 represents the reference area and represents the reference level, and $\grave{o}$ is a very small number to avoid logarithmic negativity. The head structure of FPN is responsible for predicting the position and category of equipment near the track based on the feature map output by the neck network. Due to the fact that the IOU-Aware structure can be applied to different network architectures, YOLO-R has incorporated the IOU-Aware structure into its header structure to enhance the correlation between detection credibility and location accuracy. The prediction formula for IOU-Aware is shown in equation (3).

$$IOU_{pred} = \sigma(conv_{3\times3}(feature)) \tag{3}$$

IOU_{pred} represents the predicted position of trackside equipment. σ represents the sigmoid activation function, which is utilized to limit the range of output values between 0 and 1. $\mathrm{conv}_{3\times3}$ represents the operation of convolving 3×3. The final score calculation function of IOU-Aware is shown in equation (4).

$$score_{final} = \alpha \cdot cls_{score} + (1-\alpha) \cdot IoU_{pred} \tag{4}$$

In equation (4), $score_{final}$ represents the score used for non maximum suppression and average accuracy calculation, α is a weight parameter used to balance classification score and predicted IOU value, and cls_{score} represents the category score output in the classification task. CIOULoss adds considerations for center point distance and aspect ratio on the basis of traditional IoU, which makes the loss function not only focus on overlapping areas, but also consider the distance and shape similarity between the predicted box and the real box. Therefore, YOLO-R adopts CIOULoss as the loss function to directly optimize the IOU values of the predicted and real boxes, to further raise the accuracy of position regression. The calculation method of CIOULoss is denoted in equation (5).

$$L_{CIOU} = L_{IOU} - \frac{\rho^2}{c^2} - v \cdot \delta \tag{5}$$

L_{CIOU} represents the loss function of CIOU. ρ^2 represents the square of the distance between the predicted box and the center point of the real box. c^2 denotes the square of the minimum diagonal length of the bounding rectangle. v represents the consistency measure of aspect ratio. δ is a regulatory factor utilized to balance the effects of aspect ratio. The calculation formula for ρ^2 is shown in equation (6).

$$\rho^2 = \frac{(x_{c2} - x_{c1})^2 + (y_{c2} - y_{c1})^2}{4} \tag{6}$$

(x_{c1}, y_{c1}) and (x_{c2}, y_{c2}) denote the coordinates of the center points of two bounding boxes, respectively. The calculation method of v is denoted in equation (7).

$$v = \left(\frac{4}{\pi^2}\right)\left(\arctan\left(\frac{w_2}{h_2}\right) - \arctan\left(\frac{w_1}{h_1}\right)\right)^2 \tag{7}$$

w_1, h_1 and w_2, h_2 represent the width and height of two bounding boxes, respectively. The calculation method of δ is denoted in equation (8).

$$\delta = \frac{v}{v - L_{IoU} + (1+\tau)} \tag{8}$$

τ represents a very small number used to avoid situations where the denominator is zero. YOLO-R utilizes CIOULoss to comprehensively consider overlap area, center point distance, and aspect ratio, enabling YOLO-R to converge faster during training.

2.2. Establishment of trackside equipment recognition and detection model based on YOLO-R algorithm

The study optimized the key structural aspects of the YOLO-R algorithm to raise the detection accuracy of small-sized targets on trackside equipment, laying the foundation for the position detection, numbering recognition, and model recognition of trackside equipment and its components. To complete the detection of trackside equipment, it is necessary to add modules such as image acquisition, data transmission, and data processing to build the TEID model. The structure of the identification and detection model for trackside equipment is shown in Figure 4.

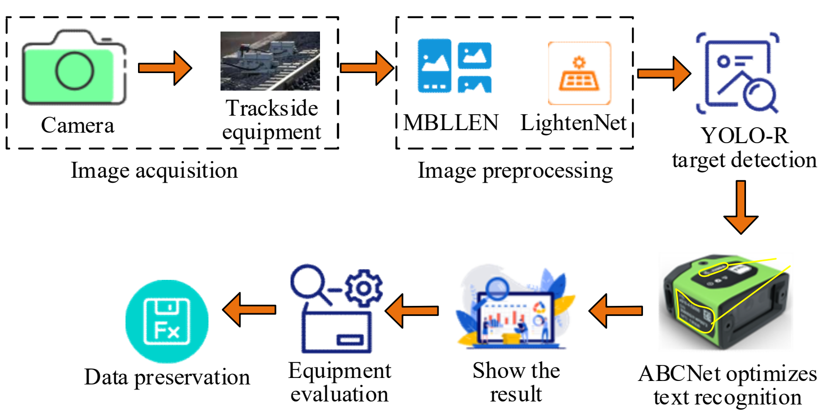

Fig. 4. Structure of TEID model

In Figure 4, TEID mainly consists of image acquisition, image preprocessing, information extraction, result analysis, and data storage modules. The image acquisition module serves as the input end of the model and is responsible for capturing real-time video or image data of high rail equipment. LightenNet is a trainable convolutional neural network used for enhancing low light images, while MBLLEN is a deep network based on ray adjustment. Therefore, image preprocessing uses LightenNet combined with MBLLEN to improve image quality. The architecture of image preprocessing is shown in Figure 5.

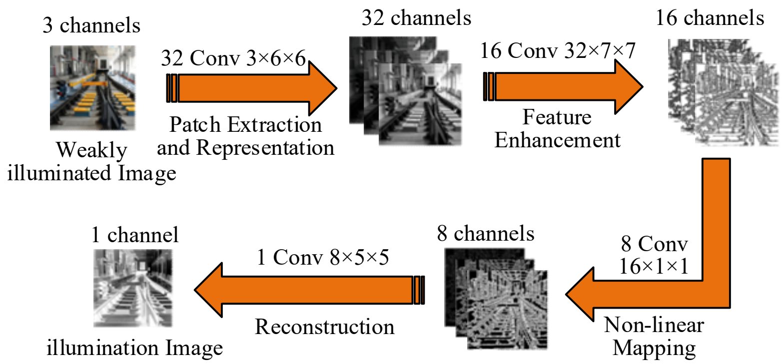

Fig. 5. The architecture of image preprocessing

The image preprocessing architecture is mainly divided into three modules: layer decomposition, reflectance restoration, and lighting adjustment, aiming to eliminate degradation in the image and learn mapping functions to meet the lighting needs of different users. The image is subjected to methods such as color balance, histogram equalization, Gaussian blur, etc. to reduce noise and improve contrast. Finally, the image is sharpened, deblurred, and color enhanced to improve its quality. The calculation method of the mapping function for extracting light rays using LightenNet is shown in equation (9).

$$\begin{cases} F_1(P) = \max(0, W_1 * P + B_1) \\ W_1 = n_1 \times f_1^2 \end{cases} \tag{9}$$

F_1 represents the mapping function, P represents the input image block, and W_1 denotes the weights of the filter. f_1 denotes the spatial support of the filter and n_1 is the number of filters. B_1 represents the filter bias term of an n_1 dimensional vector, with each element associated with a filter. $*$ stands for convolution operation. $\max(0, x)$ denotes a modified linear element used to accelerate training convergence and improve performance. The weights and bias terms of the filter are obtained through the process of supervised learning, whereby the mean square error loss function is minimized. The expression for minimizing the mean square error loss function is denoted in equation (10).

$$L(\theta) = \frac{1}{N}\sum_{i=1}^{N}\left\| F(P_i;\theta) - illu_i \right\|^2 \tag{10}$$

θ represents the set of weights and bias terms of the filter, and $L(\theta)$ represents the corresponding loss function. N represents the amount of image blocks in the training batch, P_i denotes a weak light image block, $illu_i$ is the lighting block corresponding to P_i, and F represents the learned mapping function. The calculation method for image gamma correction is shown in equation (11).

$$L'(x) = L(x)^{\gamma} \tag{11}$$

$L(x)$ represents the estimated illumination map, and $L'(x)$ represents the gamma corrected illumination map. γ is 1.7, which is a heuristic value. The region loss function of the image is denoted in equation (12).

$$\begin{aligned} L_{\text{Region}} &= w_L \cdot \frac{1}{m_L n_L} \sum_{i=1}^{m_L} \sum_{j=1}^{n_L} \left(\frac{E_L(i,j) - G_L(i,j)}{k} \right) \\ &+ w_H \cdot \frac{1}{m_H n_H} \sum_{i=1}^{m_H} \sum_{j=1}^{n_H} \left(\frac{E_H(i,j) - G_H(i,j)}{k} \right) \end{aligned} \tag{12}$$

L_{Region} represents the region loss function, $E_L(i,j)$ means the low light region of the enhanced image, and $G_L(i,j)$ denotes the low light region of the Label image. $E_H(i,j)$ represents other regions of the enhanced image, and $G_H(i,j)$ represents other regions of the Label image. w_L and w_H represent corresponding weight coefficients, F $w_L = 4$, $w_H = 1$, which is used to balance the loss contributions of different regions. m_L and n_L represent the dimensions of weak light areas, m_H and n_H represents the dimensions of other areas. k represents a constant used for normalization. The processed image is detected by YOLO-R for trackside device information in the image. Due to the ability of Bezier curves to form text boxes of any shape without adding too many parameters, therefore, the TEID model adopts ABCNet for specialized optimization of the collection of track equipment numbers. The principle of ABCNet is shown in Figure 6.

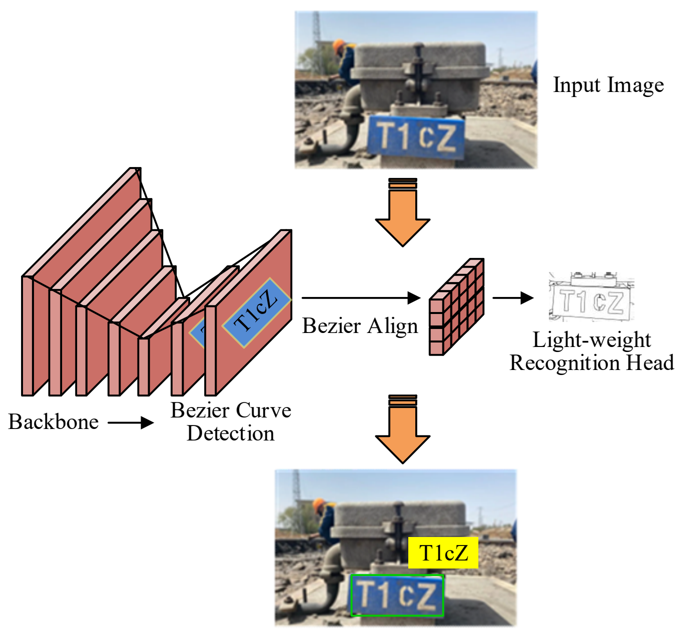

Fig. 6. Schematic diagram of ABCNet

In Figure 6, ABCNet, as an end-to-end trainable framework, can be used to recognize scene texts of any shape. ABCNet uses Bezier curves to parametrically represent text regions of any shape. The Bezier curve is a parametric curve based on Bernstein polynomials, calculated as shown in equation (13).

$$c(t) = \sum_{q}^{a=0} b_i \cdot B_{a,q}(t) \tag{13}$$

q denotes the degree of the Bezier curve and denotes the a th control point. $B_{a,q}(t)$ stands for Bernstein polynomial, which is sufficient to cover most arbitrary shaped scene texts for cubic Bezier curves $(q = 3)$. The BezierAlign layer in ABCNet is used to accurately extract convolutional features of text instances of any shape, enabling the TEID model to accurately predict text of any shape. This alignment process is similar to ROI-Align in object detection, which allows for the direct extraction of text region features from image features without the need for repeated calculations. After detecting text regions and extracting features, ABCNet uses a lightweight recognition network to recognize text content. This recognition branch utilizes features extracted from the BezierAlign layer for character level recognition. Next, the TEID model will display various information of the detected devices, and the staff will determine whether there are abnormalities and handle the devices that need maintenance. Finally, all detection and recognition results, as well as personnel handling records, will be stored for future queries, analysis, and maintenance.

3. Result

3.1. Analysis of YOLO-R's image recognition performance

To effectively analyze the performance of YOLO-R, a high-quality experimental platform was set up and the TAO Railway Dataset and UNLV Railway Dataset datasets were used. The TAO Railway Dataset contains a large number of railway images and videos, including various elements such as railway switches, tracks, signals, cables, etc. The UNLV Railway Dataset is a dataset containing over 1200 high-resolution railway images, including various railway scenes and elements. The images in these datasets also include various weather and lighting conditions, making them suitable for training and performance analysis of YOLO-R. The parameters of the experimental platform and YOLO-R are denoted in Table 1.

Table 1. Parameters of the experimental platform and YOLO-R

Experimental platform	
CPU	Intel Core i5-12400F
GPU	NVIDIA GeForce RTX 2080Ti
Memory	32GB
Storage	1TB SSD
Operating system	Windows10
YOLO-R Parameters	
Backbone network	ResNet50
Input size	640 pixels
Parameters (Param)	25.3MB
FLOPs	102.1 billion
Loss function	CIOULoss
Learning rate	0.01

The comparative algorithms used in the experiment were YOLOv3, YOLOv10, and EfficientDet algorithms. The range of loss function values is [-1,1], where 1 represents a perfect prediction. Accuracy represents whether the algorithm can accurately detect images in the dataset. Latency represents the detection speed at which the algorithm processes each image. The algorithm's performance indicators for images are Peak Signal-to-Noise Ratio (PSNR) and Structural Similarity Index (SSIM). The larger the PSNR, the smaller the image distortion. The range of SSIM values is [-1,1], and the closer it is to 1, the higher the image similarity. Mean Absolute Error (MAE) is a commonly employed metric to assess the accuracy of an algorithm in predicting images. The larger the value, the greater the prediction error. The amount of iterations during the training was 100, and the loss function values and accuracy of each algorithm throughout the entire iteration are denoted in Figure 7.

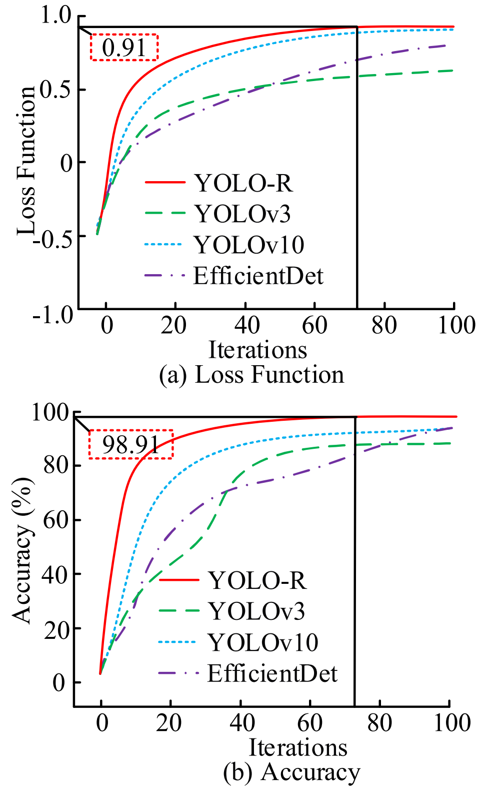

Fig. 7. The loss function values and accuracy of each algorithm

According to Figure 7 (a), when the amount of iterations was 72, the loss function value of YOLO-R was 0.91. At this point, the loss function value of YOLOv3 was 0.48, YOLOv10 was 0.89, and EfficientDet was 0.68. The loss function of YOLO-R was the closest to 1 among all algorithms, and the predicted box and the true box basically overlapped. In Figure 7 (b), the accuracy of each of the algorithms also increased with the increase in the iteration times. When the number of iterations was 72, the accuracy of YOLO-R was 98.91%, YOLOv3 was 83.78%, YOLOv10 was 93.17%, and EfficientDet was 80.58%. From this, YOLO-R could accurately detect images in the dataset, with an accuracy improvement of 5.13% compared to the unimproved YOLOv3. Throughout the testing process, the average PSNR, SSIM, Latency, and MAE of each algorithm are indicated in Table 2.

Table 2. The test results of each algorithm on each index of image detection

Algorithm	PSNR avg (db)	SSIM avg	Latency (ms)	MAE (%)
YOLO-R	67	0.94	0.57	1.09
YOLOv3	42	0.87	1.24	8.38
YOLOv10	55	0.91	0.89	3.31
EfficientDet	58	0.92	1.02	3.87

According to Table 2, the YOLO-R algorithm performed the best in all indicators, with an average PSNR of 67dB and an average SSIM of 0.94, indicating a high similarity between its detection results and the true values, and excellent image quality. The time delay of YOLO-R was 0.57ms, which was the shortest among all algorithms, indicating that its image detection speed was very fast. The MAE of YOLO-R was 1.09%, with the smallest prediction error, further confirming its high-precision detection capability. In contrast, the YOLOv3 algorithm performed poorly on PSNR and SSIM, with values of 42dB and 0.87, respectively. The time delay was 1.24ms and the MAE was 8.38%, which was the highest among all algorithms, indicating that its detection accuracy and speed were not as good as

YOLO-R. YOLOv10 showed some improvement in PSNR and SSIM, reaching 55dB and 0.91 respectively, but the time delay increased to 0.89ms, and the MAE was relatively high at 3.31%. EfficientDet performed well in PSNR and SSIM, with 58dB and 0.92 respectively, a time delay of 1.02ms, and an MAE of 3.87%. Its overall performance was also lower than YOLO-R. In summary, the YOLO-R algorithm not only had fast detection speed, but also high detection accuracy and excellent image quality.

3.2. Performance analysis of TEID model

As the foundation of the TEID model, the YOLO-R algorithm outperformed the previous YOLOv3 algorithm and the newly proposed YOLOv10 and EfficientDet algorithms in various aspects. To apply the YOLO-R algorithm to the actual detection of trackside equipment, modules such as image acquisition and data processing were added to the research. In the experimental analysis process, the research used the Neural Network Fusion Model-based Intelligent Detection of Foreign Objects in Railway Catenary (NNFM-IOD), Convolutional Network-based Railway Foreign Body Intelligent Detection Model (CNN-RFBID), and YOLOv8-based track detection model as comparative models to comprehensively compare the various indicators of the models. In the process of identifying trackside equipment on a certain section of railway, the accuracy and average recognition time of each model for different types of equipment are shown in Figure 8.

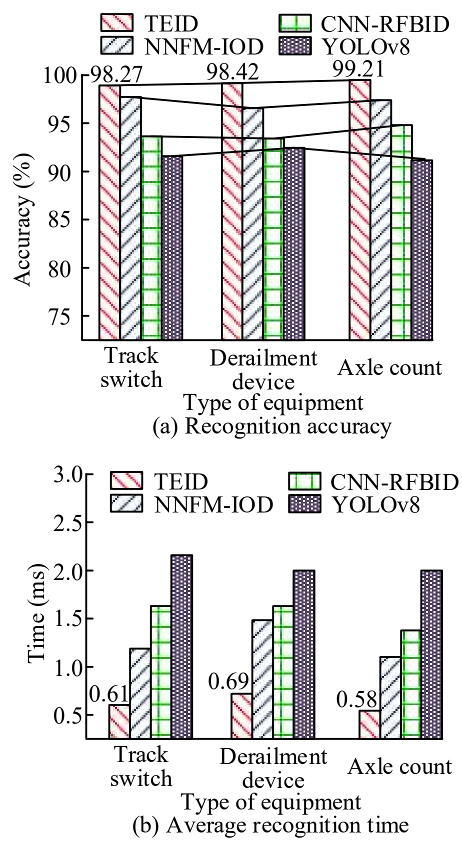

Fig. 8. The recognition accuracy and average recognition time of each model for different types of equipment

In Figure 8 (a), the TEID model had a high recognition accuracy due to its enhanced detection capability for small devices by optimizing the neck structure. The TEID model had recognition accuracies of 98.27%, 98.42%, and 99.21% for point machines, derailers, and axle counters, respectively, which were significantly higher than the NNFM-IOD model's 97.57%, 97.02%, and 97.29%. This indicated that the TEID model had higher detection accuracy, especially in the recognition of axle counting equipment, with more obvious advantages. In Figure 8 (b), the average recognition time of the TEID model was 0.61ms, 0.69ms, and 0.58ms on the switch machine, derailer, and axle counter, respectively. Compared with the NNFM-IOD model's 1.21ms, 1.49ms, and 1.02ms, the TEID model exhibited faster processing speed. This indicated that the TEID model had high real-time performance while ensuring high accuracy, which was particularly important for trackside equipment detection scenarios that require fast response. The TEID model preprocessed the collected images and also improved the detection accuracy of the model for trackside equipment. Examples of image preprocessing effects for each model are shown in Figure 9.

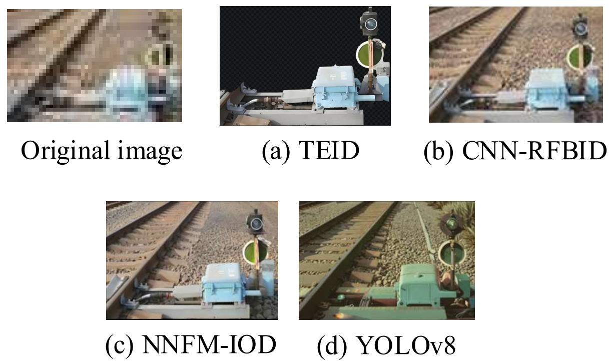

Fig. 9. Examples of image preprocessing effect of each model

In Figure 9, the TEID model not only processed images for high-definition, but also eliminated irrelevant backgrounds, improving the speed and accuracy of device recognition. However, NNFM-IOD and CNN-RFBID only sharpened the original image to make it appear clearer. Although the image processed by YOLOv8 was clearer, there was a loss of device number information, which can easily cause false positives. The TEID model has excellent performance in processing images. To analyze their actual usage ability, the resource utilization rate and image processing speed of each model on the computer during a continuous 24-hour usage process are shown in Figure 10.

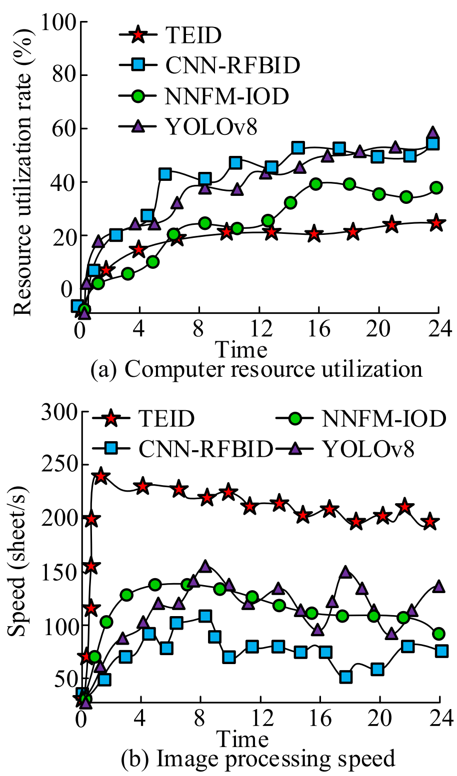

Fig. 10. The resource utilization rate and image processing speed of each model on the computer

In Figure 10 (a), with the increase of time, the resource utilization rate of the TEID model on the computer increased, but remained below 22%. The situation of YOLOv8 and CNN-RFBID models was similar, with a computer resource utilization rate of 58%. The computer resource utilization rate of the NNFM-IOD model, although initially low, increased to 38% over time. From Figure 10 (b), the TEID model's image processing speed ultimately stabilized around 200 frames per second, which was better than YOLOv8's 135 frames per second. As the running time increased, the computer temperature rose, and the speed of TEID model processing images would be affected to some extent, but it still maintained a relatively high speed. From this, the TEID model occupies relatively low computer resources in practical use and can maintain fast image processing speed for a long time.

4. Conclusions

To improve the recognition and detection efficiency of trackside equipment, YOLO-R was used as the basis to construct a TEID model for trackside equipment recognition and detection. The TEID model aimed to improve the detection accuracy and real-time response capability of small devices by optimizing the network structure and introducing an image preprocessing module. The result analysis showed that the TEID model had a recognition accuracy of 98.27% in the switch machine, an average recognition time of 0.61ms, a computer resource utilization rate of less than 22%, and a processing speed of more than 200 images per second, which was better than the comparison model. In summary, the TEID model performs well in the detection of trackside equipment, and can quickly and accurately detect different types of trackside equipment while maintaining low computational resource consumption while ensuring high accuracy. Although the TEID model has made significant progress in identifying trackside devices, its recognition performance for other scenarios still needs further improvement. In the future, image preprocessing algorithms will be optimized to improve the detection capability of TEID models in different environments. At the same time, it will consider to introduce more multimodal data for training to enhance the model's generalization ability and robustness, achieving higher performance and wider applicability.

References

[1] Rantatalo, M., Chandran, P., Thiery, F., Odelius, J., Gustafsson, C., Asplund, M., & Kumar, U. (2023). Evaluation of Measurement Strategy for Track Side Monitoring of Railway Wheels. Applied Sciences, 13(9), 5382.

[2] Peng, X., Zeng, J., Wang, Q., & Zhu, H. (2023). Research on an identification method for wheelset coaxial wheel diameter difference based on trackside wheelset lateral movement detection. Sensors, 23(13), 5803.

[3] Kunisaki, A., Fujita, H., Nomura, T., & Ishii, T. (2021). Lifetime Evaluation Method for Electronic Equipment of Wayside Signalling Systems. Quarterly Report of RTRI, 62(2), 110-117.

[4] Paś, J., Rosiński, A., Wetoszka, P., Białek, K., Klimczak, T., & Siergiejczyk, M. (2022). Assessment of the Impact of Emitted Radiated Interference Generated by a Selected Rail Traction Unit on the Operating Process of Trackside Video Monitoring Systems. Electronics, 11(16), 2554.

[5] Gao, L., Jiu, Y., Wei, X., Wang, Z., & Xing, W. (2020). Anomaly detection of trackside equipment based on GPS and image matching. IEEE Access, 8, 17346-17355.

[6] Carnevali, L., Fantechi, A., Gori, G., Parri, J., Pieralli, M., & Sampietro, S. (2021). A heuristic approach for predictive diagnosis of wheel wear based on low-cost track-side equipment. INGEGNERIA FERROVIARIA, 5-27.

[7] Bureika, G., Levinzon, M., Dailydka, S., Steisunas, S., & Zygiene, R. (2019). Evaluation criteria of wheel/rail interaction measurement results by trackside control equipment. International journal of heavy vehicle systems, 26(6), 747-764.

[8] Kowalik, R., & Sadowski, E. (2020). Reliability model of the RTC System with trackside equipment equipped with a Peltier cell. Journal of civil engineering and transport, 2(2), 98-108.

[9] Hao, W. E. I. (2024). Research on Aerodynamic Effect on Trackside Monitoring Equipment Safety for High-speed Railway. Railway Investigation & Surveying, 50(5).

[10] Zhang, J., Xu, L., Shen, T., & Luo, J. (2022). Energy harvesting approach for trackside health monitoring devices in railroads. IET Electric Power Applications, 16(1), 100-111.

[11] Ulianov, C., Hadaš, Z., Hyde, P., & Smilek, J. (2020). Novel energy harvesting solutions for powering trackside electronic equipment. Sustainable Rail Transport, 229-255.

[12] Zhiwei, B., Shenlin, Y., Wei, Z., & Lanxin, L. (2021). Research on Corrosion Life Evaluation Method of Trackside Equipment in High Salt and High Humidity Environment. Railway Signalling & Communication Engineering, 18(3), 12.

[13] Xing, M., Ding, H., Ao, Q., Huang, B., Ren, X., & Ge, S. (2023, December). Design of Safe Trackside Equipment Driving and Control System. In 2023 5th International Conference on Electrical Engineering and Control Technologies (CEECT) (pp. 421-425). IEEE.

[14] Shaikh, M. Z., Ahmed, Z., Chowdhry, B. S., Baro, E. N., Hussain, T., Uqaili, M. A., ... & Shah, A. A. (2023). State-of-the-art wayside condition monitoring systems for railway wheels: A comprehensive review. IEEE Access, 11, 13257-13279.

[15] Guo, X., Wei, X., Guo, M., Wei, X., Gao, L., & Xing, W. (2020, December). Anomaly detection of trackside equipment based on semi-supervised and multi-domain learning. In 2020 15th IEEE international conference on signal processing (ICSP) (Vol. 1, pp. 268-273). IEEE.

[16] Yin, M., Li, K., & Cheng, X. (2020). A review on artificial intelligence in high-speed rail. Transportation Safety and Environment, 2(4), 247-259.

[17] Liu, Z., Jerresand, A., Diamant, M., Zarov, F., Berg, M., Bonnevier, F., & Malas, J. (2024). Application of smart wayside object controllers to railway signalling systems for decarbonisation. Proceedings of the Institution of Mechanical Engineers, Part F: Journal of Rail and Rapid Transit, 238(3), 338-346.

[18] Zhang, Z., Zaman, A., Xu, J., & Liu, X. (2022). Artificial intelligence-aided railroad trespassing detection and data analytics: Methodology and a case study. Accident Analysis & Prevention, 168, 106594.